Applied Surface Science 628 (2023) 157350

Contents lists available at ScienceDirect

Applied Surface Science

journal homepage: www.elsevier.com/locate/apsusc

Full Length Article

Hyper-conjugated polyaniline delivering extraordinary electrical and electrochemical properties in supercapacitors

Yihan Wang [a,b], Xiang Chu [b], Hongrui Zhang [b], Cheng Yan [b], Guo Tian [b], Weiqing Yang [b], Xiangrong Chen [a], Haitao Zhang [b,*]

[a] Institute of Atomic and Molecular Physics, Sichuan University, Chengdu 610065, China
[b] Key Laboratory of Advanced Technologies of Materials, Ministry of Education, School of Materials Science and Engineering, Southwest Jiaotong University, Chengdu 610031, China

ARTICLE INFO

Keywords:
Conjugated polymers
Hyper-conjugated effect
Electronic properties
Electrochemical properties
Supercapacitors

ABSTRACT

Conjugated polymers promise extremely-high theoretical supercapacitance to develop large capacitive storage devices. Existing conjugated polymers commonly realize their < 20% supercapacitance due to inferior electronic and electrochemical activities. Here we report hyper-conjugated effect to minimize energy level difference and carrier migration barrier in copolymerized polyaniline (PANI), a typical supercapacitive material. The hyper-conjugated effect efficiently promotes the elongation of conjugation system and the delocalization of π electrons. The largely increased number of free carriers in combination with the expanded range of carrier mobility guarantee 800% increments in electrical conductivity. Tests of symmetric supercapacitors with hyper-conjugated PANI show a high specific capacitance of 512 F g^{-1}, excellent rate-capability and long-term cyclability. This work paves the way for designing conjugated polymers with remarkable electronic and electrochemical properties.

1. Introduction

Energy and environmental issues have become a hot spot and challenge in the forefront of society and academia[1–3]. Energy storage devices — supercapacitors, have developed rapidly in power vehicles, portable devices, wearable flexible displays and other fields due to their advantages of high power density, fast charging and discharging rate and wide operating temperature range[4–8]. As one of the main factors affecting the performance of supercapacitors, conjugated polymer electrode materials combine the advantages of traditional polymer materials and organic conductors, thus possessing high charge storage capacitance and mechanical flexibility[9–12]. In such supercapacitive materials, the main charge storage mechanism is attributed to faradaic redox reactions occurring at or near the surface of the electrode materials[13].

Conjugated polymers, such as polyaniline (PANI), show supercapacitance characteristics in nature, so they share a high theoretical specific capacitance up to 2000 F g^{-1}[14]. However, the actual capacitance of conjugated polymers is still far behind the theoretical value. In this regard, researchers improve its electrochemical activity by means of designing nano-structure, compositing with carbon materials, and constructing three-dimensional network[15–18]. However, the operation process is rather complicated and the effect is very limited, most of which deliver a specific capacitance of 100–300 F g^{-1}[19–21].

Therefore, an alternative strategy based on introduction of secondary phase during polymerization has been proposed to boost the electrochemical properties of conjugated polymer-based supercapacitors [22,23]. It has been reported that adding a small amount of p-phenylenediboronic acid, in the polymerization process can form a longer polymer chain with less entangling, which can significantly improve the specific capacitance and the energy density of PANI-based supercapacitors[24]. Although the specific capacitance and the energy density of conjugated polymer-based supercapacitors can be increased to some extent by introducing the second phase material, there are still some obstacles need to be solved or clarified[25,26]. The first problem lies that the introduction of inactive dopants cannot contribute to the capacitive behavior and therefore results in low specific capacitance. The second problem is that the mechanism of introducing the secondary phase in the synthesis process needs to be further clarified. And the last one is that it is still unclear to the relationship between the electrical properties and the electrochemical properties after introducing the secondary phase.

* Corresponding author.
E-mail address: haitaozhang@swjtu.edu.cn (H. Zhang).

https://doi.org/10.1016/j.apsusc.2023.157350
Received 24 February 2023; Received in revised form 8 April 2023; Accepted 21 April 2023
Available online 25 April 2023

Herein we firstly propose an active molecular copolymerization (3-amino benzyl alcohol, 3-ABA in this work) to modify the molecular chains of conjugated polymers, using pure polyaniline (p-PANI) as an example. By introducing more amino groups and hydroxyl groups contained on benzene rings, the PANI molecular chains are extended to achieve higher electrochemical activity. Except from the π-π conjugated effect in p-PANI, the C–H σ bonds interact with the delocalized π bonds of benzene ring, and therefore forms an additional hyper-conjugated effect (termed as hyper-conjugated PANI, hc-PANI). We proved that this hyper-conjugated effect efficiently increases the electrical conductivity by 800%. And it is in combination with hyper-conjugated and hydrogen bond effect to enable electrochemical performance, hc-PANI based supercapacitors show a high specific capacitance of 521 F g^{-1}, a remarkable 50% larger than that of p-PANI.

2. Experimental

2.1. Materials

Aniline and 3-aminobenzyl alcohol (3-ABA) were purchased from Aladdin (Shanghai, China). Hydrochloric acid and ammonium persulfate (APS) were purchased from Kelong chemical reagent factory (Chengdu, China). All the reagents were analytical grade.

2.2. Synthesis of hc-PANI and p-PANI

The 0.4564 g ammonium persulfate in 2 mL deionized water solution was prepared in advance and used as the initiator (solution A). Then, adding 0.062 g 3-aminobenzyl alcohol into 2.03 mL 6 M HCl solution. As the 3-ABA is completely dissolved, 0.14 mL aniline monomers were added and mixed well (solution B). For complete cooling, solutions A and B were put in an ice water bath for 20 min. Next, the solution A was added into solution B followed by mixing solutions with stirring rapidly for 5 min. After that, the mixed solutions were let stand on ice water bath for more than 12 h to form a hydrogel-like substance. With further permeation, filtration, washing, and desiccation, the product recorded as hc-PANI was prepared. According to different ratios of aniline to 3-ABA monomers, hc-PANI-1 (1:3), hc-PANI-2 (2:2), and hc-PANI-3 (3:1) were synthesized, respectively. For comparing, pure PANI (4:0) was also prepared in accordance with the same procedures except from no addition of 3-ABA.

2.3. Preparation of supercapacitor electrode and flexible supercapacitors

To prepare supercapacitor electrodes for three-electrode tests, polyethylene terephthalate (PET) film was employed as the flexible substrate. Gold thin film was then evaporated onto PET film and served as the current collector through magnetron sputtering. Sequentially, p-PANI and hc-PANI dispersed into deionized water were respectively sprayed onto the current collector to form the film electrodes. For preparing the device of supercapacitors, a spraying technology was employed to attach the active materials on Au current collectors with the help of a pattered mask. After removing the mask, interdigital electrodes were formed. Through coating with PVA/H_2SO_4 gel electrolyte and encapsulating with polydimethylsiloxane (PDMS), flexible supercapacitors were finally prepared.

2.4. Characterizations

Gel permeation chromatography (GPC, OMNISEC, Malvern Panalytical) method was used to confirm the average molecular weight of the samples. Nuclear Marnetic Resonance (NMR) characterization was carried out on an AVANCE III HD instrument (Bruker). Scanning Electron Microscopy (SEM, JSM-7800F Prime) and Transmission Electron Microscopy (TEM, JEOL JEM-2100F) were used to detect the microstructure and morphology of the samples. The crystallinity was characterized by X-ray Diffraction (XRD, PANalytical X'Pert). The elements and their chemical atmosphere were analyzed by X-ray Photoemission Spectroscopy (XPS, Thermo Scientific™ K-Alpha™). The spectral response of the materials was analyzed by Fourier Transform Infrared Spectroscopy (FTIR, Nicolet iS10) and Raman spectrum (Horiba Lab RAM HREvolution). For measuring the electrical conductivity by a four-point probe (RTS-9, China), the powder materials were pressed into 0.3–1.0 mm thick discs with a diameter of 15 mm using a tablet press. UV–vis (UV2310II, China) spectra were measured with using N-methylpyrrolidone solvated p-PANI and hc-PANI solutions. The relative permittivity was measured on Broadband Dielectric Spectrometer (Novocontrol). Ultraviolet Photoelectron Spectroscopy (UPS) was tested by Thermo Fischer, ESCALAB Xi+ (US) under vacuum degree of $8 \times l0^{-10}$ Pa, working voltage of 12.5 kV and filament current of 16 mA. He lamp is used as a monochromatic light source with photon energy of 21.22 eV.

2.5. Electrochemical properties

The electrochemical properties are mainly characterized by CHI660E electrochemical workstation (Shanghai, China). The electrochemical properties of materials are characterized by a three-electrode system, including working electrode, auxiliary electrode (platinum sheet) and reference electrode (saturated calomel electrode), and the electrolyte is 1 M H_2SO_4 aqueous solution. The test methods mainly involve cyclic voltammetry (CV), galvanostatic charge–discharge (GCD), electrochemical impedance spectroscopy (EIS) and cycle stability test. Using the impedance-potential program in the electrochemical workstation, the Mott-Schottky curves were also measured. Cyclic voltammetry test operates at a voltage range of 0–0.7 V, and the scan rate increases from 5 mV s^{-1} to 100 mV s^{-1}. The test parameters of galvanostatic charge–discharge mainly include voltage range (0–0.7 V) and current density (1–10 A g^{-1}). Electrochemical impedance spectroscopy recorded in the frequency range of 10^5 Hz to 0.01 Hz. The specific capacitance of electrochemical active materials under different current densities can be analyzed by GCD curves, so as to obtain electrochemical characteristics such as multiplier performance. The capacitances are calculated according to the following formula:

$$C_{m,GCD} = \frac{I}{m}\frac{\Delta t}{\Delta V} \quad (1)$$

Where I is discharge current, Δt is discharge time, m is the loading mass of active material, and ΔV is potential window.

$$C_{A,GCD} = \frac{I}{A}\frac{\Delta t}{\Delta V} \quad (2)$$

Where I is discharge current, Δt is discharge time, A is the effective geometrical area of the interdigital electrodes and ΔV is potential window.

2.6. Computational calculations

The structure of hc-PANI and P-Pani were optimized using density function theory (DFT) by Gaussian 09 software package. The B3LYP functional associated with 6–31 G (d, p) basis set was used for DFT calculations. The conjugated structures and energy levels of highest occupied molecular orbitals (HOMO) and lowest unoccupied molecular orbitals (LUMO) were obtained by Gaussian view. The molecular orbitals of were visualized by Multiwfn package and VMD.

3. Results and discussion

The carrier of PANI with conjugated structure is composed of bipolarons, solitons, polarons and delocalized π electrons introduced by dopants[27,28]. As it is in original state, there is a difference in energy level between π bonds of molecular orbitals because the mobile π electrons needs to cross the energy level to form carriers, which hinders its

migration in the internal molecular chain of the conjugated PANI. After copolymerization, the energy level of the π electrons would be delocalized, leading to the reduction of energy level difference between the energy bands. This process facilitates to decline the energy barrier in carrier migration.

For solving this difference, an electrochemical active molecule of 3-ABA was introduced to generate long chain hc-PANI with hyper-conjugated and hydrogen bond effect from short chain pure polyaniline (p-PANI) (Fig. 1a-b). After incorporation of 3-ABA molecules, they polymerized into the molecular chains of PANI, and hence elongated the molecular chains. The gel permeation chromatography (GPC) measurement demonstrated that several kinds of average molecular weight are larger in hc-PANI than p-PANI (Table S1). Specifically, the weight average molecular (M_W) of hc-PANI is 3760 while it is 3311 of p-PANI (Fig. 1c).

Solid-state H1-NMR of p-PANI and hc-PANI are shown in Fig. 1d. Because of the limited resolution in solid-state H1-NMR, there is a very broad peak corresponding to aromatic proton (Fig. 1d). Due to the ring current effect of the benzene ring, the corresponding peaks at $\delta = 8.2$ and $\delta = 10.3$ are aromatic proton, while in hc-PANI, the peaks at $\delta = 10$ are significantly enhanced, indicating that alcoholic hydroxyl group, which provides the σ-π hyper-conjugated effect, has been successfully inserted into the benzene ring[29].

The lone pair electron in the P orbital of the N atom forms the p-π conjugated system with the π electron in the connected benzene ring, and since the interaction between C–H σ bond in 3-ABA and the π orbital of benzene ring, an additional σ-π hyper-conjugated effect is generated (Fig. 1e-f). This hyper-conjugation achieves the purpose of further expanding the delocalization ability of π electrons and increasing the transferable range of carriers[30]. The conjugate structure of p-PANI and hc-PANI is obtained by Gaussian calculation[31]. In p-PANI, electrons of N atom have no delocalization in Fig. 1g-h, while in hc-PANI (Fig. 1i-j), the π orbital in benzene ring overlaps with p orbital on the adjacent N atom to form obvious p-π conjugated system (red circle). The σ bond of C atom provided by the alcohol hydroxyl group on 3-ABA also forms weak hyper-conjugated (purple circles) with the π orbital in benzene ring.

The molecular vibrations were probed to detect the microstructure of hc-PANI. As shown in Fig. 2a, O–H stretching vibration at 3477 cm^{-1} is apparently observed in hc-PANI while it is absence in p-PANI[32]. Hence, hydrogen bonds are formed through introducing 3-ABA molecules as above discussed. The oxygen atom in the alcohol hydroxyl group of 3-ABA forms a hydrogen bond effect with the hydrogen atom in the amino group of polyaniline molecular chain. The peak near 3228 cm^{-1} is related to N–H stretching vibration in emerald imine salt (Fig. S1). In the fingerprint region (Fig. 2b), quinone structure N = Q = N stretching vibration in emerald imine salt occurs at 1577 cm^{-1} while at 1494 cm^{-1} corresponds to benzene structure N-B-N stretching vibration in emerald-imine salt[33]. The other two peaks located at 1305 cm^{-1} and 1249 cm^{-1} are assigned to be C-N and C = N stretching vibration of benzene ring/aromatic amine in PANI. In addition, another obvious absorption peak at 819 cm^{-1}, corresponding to the out-of-plane bending vibration of C–H [34].

Raman spectra (Fig. 2c) show that the out-plane C–H waging vibration and deformation of benzene ring appears at 418 cm^{-1} and 813 cm^{-1} while at 1170 cm^{-1}, in-plane C–H bending vibration of quinone ring is also observed. The stretching vibration of C-N bond in dipole structure shares a peak at 1334 cm^{-1}. Another weak peak at 522 cm^{-1} is assigned to out-plane C-N-C torsion vibration and it becomes weak in hc-PANI. The peak at 1344 cm^{-1} is assigned to the C–N^+ stretching

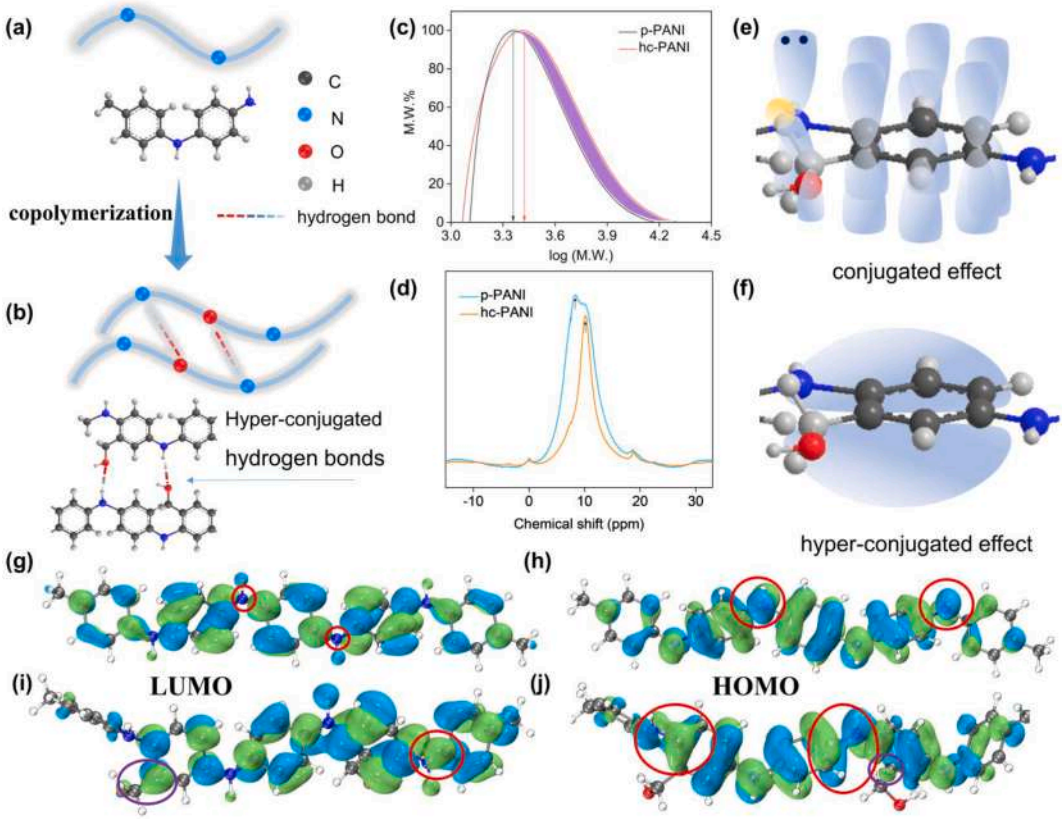

Fig. 1. Formation schematic diagram of hyper-conjugated PANI (hc-PANI). Schematic illustration of short chain pure PANI (p-PANI) (a) copolymerized to form hc-PANI (b) with extended molecular chain and supramolecular hydrogen bonds. (c) Molecular weight comparison between p-PANI and hc-PANI. (d) H-NMR of p-PANI and hc-PANI. (e) p-π conjugated effect in p-PANI. (f) Additional σ-π hyper-conjugated effect in hc-PANI. Theoretical calculation of molecular orbital visualization. (g) LUMO of p-PANI, (h) HOMO of p-PANI, (i) LUMO of hc-PANI, (j) HOMO of hc-PANI.

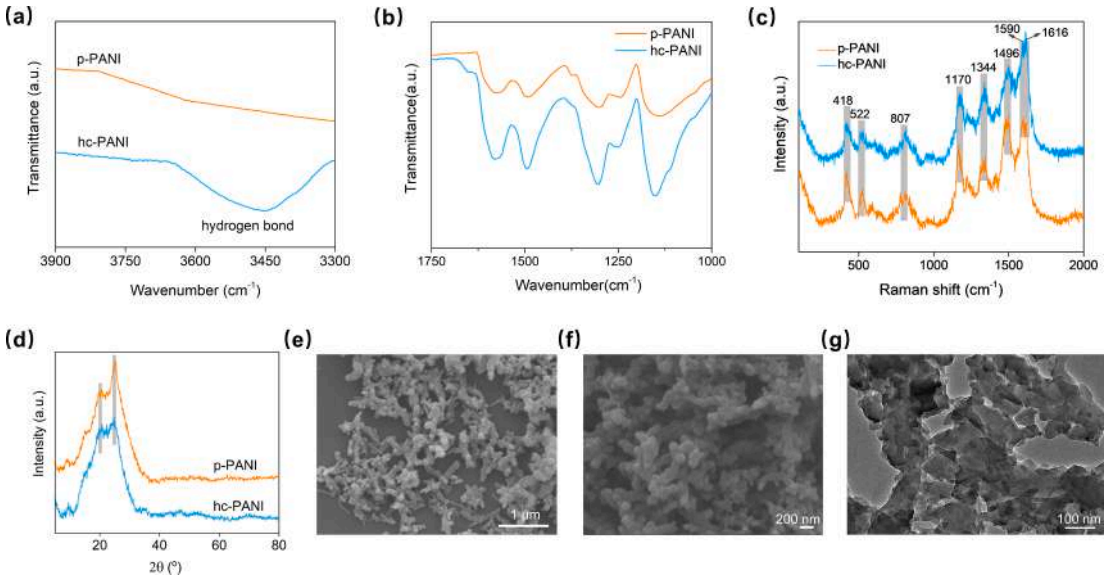

Fig. 2. Microstructure and morphology of hc-PANI. (a) Partially enlarged FTIR spectra. (b) FTIR spectra at fingerprint area of p-PANI and hc-PANI. (c) Raman spectra of p-PANI and hc-PANI. (d) XRD of p-PANI and hc-PANI. SEM of (e) p-PANI, and (f) hc-PANI. (g) TEM of hc-PANI.

vibration of more delocalized polaronic structures[35], proving the intensive formation of polarons. And it becomes stronger in hc-PANI than p-PANI, implying the generation of more polarons and bipolarons delocalized on hc-PANI after copolymerization with 3-ABA molecules [36]. The peak occurred at 1496 cm^{-1} is attributed to the stretching vibration of quinone C = N bonds. The sharp broad peak can be separated two peaks at 1590 cm^{-1} and 1616 cm^{-1} that are originated from the stretching vibration of C = C and C–C bonds. The decrease of relative

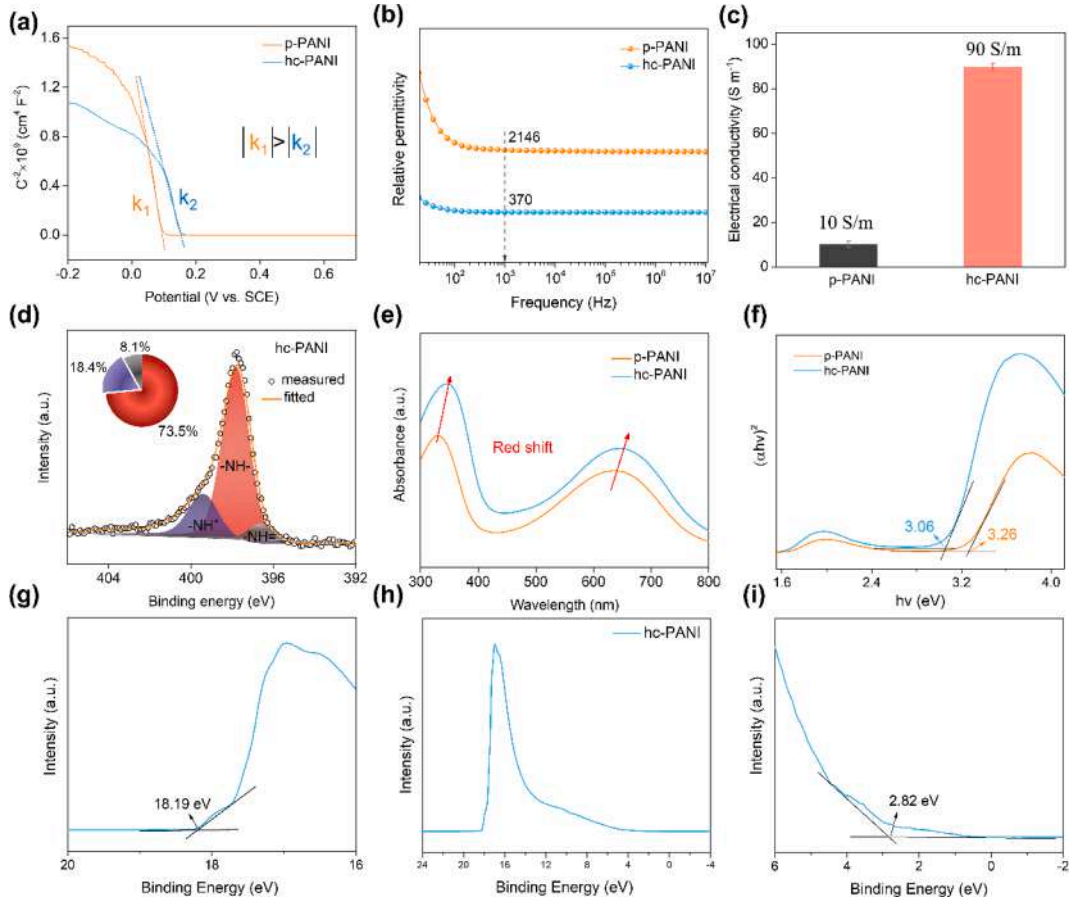

Fig. 3. The improved electronic properties of hc-PANI. Comparison of p-PANI and hc-PANI in (a) Mott-Schottky curve, (b) dielectric constant, (c) electrical conductivity. (d) XPS of hc-PANI. (e) UV–vis spectra. (f) Tauc diagram of p-PANI and hc-PANI. (g-i) UPS spectrum of hc-PANI. (g) Enlarged image of E_{cutoff}, (h) The full spectrum, (i) Enlarged image corresponding to the Fermi edge.

peak strengths for both C = N and C = C bonds implies that the strengthened delocalized effect of π electrons in hc-PANI than p-PANI because of the additional hyper-conjugated action in the former. In short, the detection of molecular vibrations implies the successful introduction of additional hyper-conjugation effect in hc-PANI.

In XRD pattern (Fig. 2d), there are diffraction peaks located at 2θ = 20.6°, 24.7°, corresponding to (0 2 0), (2 0 0) crystallographic planes, respectively[37]. These two peaks belong to the characteristic of PANI emeraldine salt in a pseudo-orthorhombic unit cell[38], confirming the original crystal structure of PANI was not damaged after 3-ABA is involved in the copolymerization. The two diffraction peaks represent the diffraction peaks produced periodically parallel to the polymer chain group and periodically perpendicular to the polymer chain group. The relative diffraction intensity of (0 2 0) crystal plane increases, indicating that hc-PANI has better crystallinity and more regular structure. Such good crystallinity and regular structure will significantly improve the electrochemical performance of polyaniline, and inhibit the volume change in the process of charging and discharging, which is an important factor for the electrode material to have excellent cycle stability and rate-capability [39].Hence, comparing with p-PANI, hc-PANI deliver enhanced conjugated effect and accordingly electrochemical properties.

The morphology of SEM between hc-PANI and p-PANI is similar (Fig. 2e-f). And SEM and TEM characterizations (Fig. 2f-g) display the short rod morphology of hc-PANI that is very common in conjugated polymers[40]. In addition, in comparison with p-PANI, hc-PANI solution show a hydrogel characteristic (Fig. S2), indicating further crosslinking in hc-PANI. We proved that 3-ABA was essential to form hydrogel-like hc-PANI (Fig. S3).

After realizing hyper-conjugated and hydrogen bond effect in hc-PANI, we will discuss that the electronic and electrochemical properties are greatly improved due to these two positive effects. Firstly, the Mott-Schottky curve was measured. As shown in Fig. 3a, the negative slope of Mott-Schottky curve for both p-PANI and hc-PANI indicates their characteristics of p-typed semiconductor. According to Mott-Schottky formula (Equation (3) [41], the absolute slope value is much smaller in hc-PANI than p-PANI (7.55 vs. 14.80), indicating that the former possesses much higher carrier concentration.

$$1/C^2 = 2/\varepsilon q N_A A^2 (V - V_{FB} - kT/e) \quad (3)$$

Where, C is space charge layer capacitance, ε is dielectric constant, q is charge quantity of element charge, N_A is carrier concentration, V is applied bias, V_{FB} is flat band potential, k is Boltzmann constant.

In combination with determining the permittivity (e) by broadband dielectric impedance spectrometer, by which the permittivity values of p-PANI are 2146 F m^{-1} and hc-PANI is 370 F m^{-1} at 1 kHz (Fig. 3b). After quantifying the other values from Mott-Schottky curves, the carrier concentrations (N_A) were determined to be 4.46 × 10^{25} cm^{-3} for hc-PANI and 3.93 × 10^{24} cm^{-3} for p-PANI, increased by an order of magnitude. Because of much higher carrier concentrations, hc-PANI exhibits 800% increment in electrical conductivity as illustrated in Fig. 3c. The average electrical conductivity of p-PANI is 10 S m^{-1}, while it is up to 90 S m^{-1} for hc-PANI. As kown to us, PANI in original state is close to the insulator. As H protons are doped into the molecular chains, the charge will transport in the whole PANI molecular chains because of the p-π conjugated effect that tremendously enhances the electrical conductivity.

Next, we revealed that the enhanced electrical properties are correlated with the increased protonation induced by additional hyper-conjugated effect. The N atoms on the PANI molecular chain are protonated to produce cations and form a quaternary ammonium salt structure with anions[42]. During the doping process by proton acids, the protonation at the N atom in imine is occurred at the first. As the dissociation of proton acids, the proton hydrogen (H^+) transfers into the molecular chains of PANI. This process makes protonation of N atom in imine and generates excited polarons with charge, which endows 10 orders of magnitude variation between PANI insulating and conducting states. In hc-PANI, this p-π conjugated effect is also retained. The deconvolution of N 1 s XPS spectra shows that the –NH^+ ratio of hc-PANI is increased from 14.6% to 18.4% (Fig. 3d and Fig. S4). In addition, XPS full-scan spectra shows the presence of O atoms belonged to 3-ABA molecules (Fig. S5), again implying the successful polymerization of hc-PANI. Moreover, the strengthened protonation in combination with improved electrical conductivity also facilitates to superior pseudo-capacitive behavior, which we will discuss later.

Additional evidence to the improved electronic properties lies to the electron transition as analyzed by UV–vis spectra (Fig. 3e). There are two strong broad absorption peaks at 330 nm and 628 nm, respectively. The former is related to π-π* transition in the benzene ring of PANI, in which electrons transit from the highest occupied molecular orbital to the lowest unoccupied molecular orbital[43]. The peak at 628 nm is aroused by the n-π* transition that is attributed to the electron transition from benzene ring to quinone ring in PANI. The absorption peak of hc-PANI occurs a slight red shift, indicating that the effective conjugated chain length becomes longer and the π electron delocalization degree increases, which proves the existence of hyper-conjugated system. Since this hyper-conjugated effect is much weaker than that of conjugated effect, the red shift is not very obvious. By converting the UV–vis spectrum into Tauc diagram (Fig. 3f), band gap values can be obtained. The band gap of p-PANI is 3.26 eV, while the hc-PANI is 3.06 eV. In general, a smaller band gap means better conductivity, which also corresponds to the previous experiments[44,45]. In order to calculate the HOMO level of hc-PANI and p-PANI, UPS tests were carried out (Fig. 3g-i). The interaction information of electrons near the Fermi level (valence shell electrons) is reflected by vacuum ultraviolet excitation of the sample. By measuring the energy distribution of valence electrons, UPS spectroscopy can obtain various information about valence electron structure, including valence band spectrum, escaped work, and ionization potential (IP) of valence electrons, etc[46]. The IP of conjugated polymer corresponds to the HOMO level, so UPS has become a common method to measure the HOMO level of organic semiconductor materials [47]. He 1 light source with an energy of 21.22 eV was used in this work, and the formula for calculating HOMO is as follows:

$$E_{HOMO} = -(IP) = -(h\nu - E_{cutoff} + E_{VB^F}) \quad (4)$$

Where, E_{HOMO} is energy levels of highest occupied molecular orbitals, IP is ionization potential of valence electrons, $h\nu$ is incident photoelectron energy, E_{cutoff} is cutoff energy of the secondary electron, E_{VB}^{F} is energy difference between valence band top and Fermi level.

The electron work function can be calculated by subtracting cutoff energy of the secondary electron from incident photoelectron energy, which represents the minimum energy required to remove an electron from the material[48]. As can be seen in Fig. 3g, the spectral line begins to rise near 18.19 eV, indicating strong secondary inelastic scattered electron emission, which can be obtain the E_{cutoff} is 18.19 eV. The Fermi edge corresponds to the position of the lowest binding energy, representing the valence band to Fermi energy[49]. It can be seen from Fig. 3i that E_{VB}^{F} is 2.82 eV. Therefore, the HOMO of hc-PANI calculated by Formula 4 is −5.85 eV. The UPS spectrum of p-PANI is shown in Fig. S6, and the HOMO of p-PANI is −5.32 eV.

$$E_g = E_{LUMO} - E_{HOMO} \quad (5)$$

Where, E_g is band gap, E_{LUMO} is energy levels of lowest unoccupied molecular orbitals.

UPS cannot measure LUMO levels because the molecule has no electrons to excite[50]. However, LUMO level can be evaluated in combination with the optical band gap measured by UV–vis. According to Formula 5, the LUMO of hc-PANI and p-PANI is −2.79 eV and −2.03 eV, respectively.

As above-discussed, hc-PANI possess electrochemical hydrogen bond effect and additional hyper-conjugated effect promoted extraordinary

electronic properties, therefore, the superior electrochemical properties of hc-PANI would be also anticipated. As shown in Fig. 4a, the cyclic voltammetry (CV) curves at different scanning rates have two obvious redox peaks within the voltage range of 0–0.7 V, supplying high pseudocapacitance for hc-PANI electrodes. The oxidation peak at 0.33 V and the reduction peak at 0.09 V correspond to the transition of fully reduced benzene structure leucoemeraldine to the intermediate oxidation state emeraldine in hc-PANI, while the oxidation peak at 0.58 V and the reduction peak at 0.38 V correspond to the transformation from the intermediate oxidation state to the full oxidation state of pernigraniline. [24] At a current density of 1 A g^{-1}, the hc-PANI electrode material could reach a high average specific capacitance of 521 F g^{-1} (Fig. 4b), while that of p-PANI is only 342 F g^{-1} (Fig. S7). We also testified the optimum electrochemical properties occurred in hc-PANI of which molar ratio of aniline to 3-ABA was 3:1 (Fig. S8). With the current density increased to 2 A g^{-1} and 5 A g^{-1}, it corresponded to 496 F g^{-1} and 478 F g^{-1}, respectively. Even if at 10 A g^{-1}, the specific capacitance still maintained about 86.9% (453 F g^{-1}), indicating excellent rate-capability (Fig. 4c). After the supercapcitors are assembled (Fig. 4d), the specific capacitance of the device is 134 F g^{-1} at the current density of 1 A g^{-1}, 123 F g^{-1} and 119 F g^{-1} at the current densities of 2 A g^{-1} and 5 A g^{-1}, respectively. As the current density is up to 10 A g^{-1}, the capacitance is 117 F g^{-1}, still showing a high capacitance retention rate of 87.3% (Fig. 4e). Therefore, even after the device is assembled, the corresponding capacitance of the hc-PANI still does not decay and has excellent rate-capability.

The device also has a good cycling stability, the capacitance retention rate can be 89.7% after 10,000 cycles (Fig. 4f). In order to explore the flexibility of supercapacitors constructed by hc-PANI nanomaterial, the electrochemical properties at different bending angles were tested (Fig. 4g). As shown in Fig. 4h by comparing CV curves at different bending angles (0°-120°), there is little difference in the curves of supercapacitors, indicating that the hc-PANI based devices have ideal flexibility. In addition, the GCD curves also show similar consistency (Fig. S9). The electrochemical performance comparison between this work and the reported work confirms that the electrode material based on hc-PANI has excellent specific capacitance, cycling stability and rate-capability (Table S2)[51–55].

The average thickness obtained by cross-section SEM images is 4.79 μm (Fig. S10). At a current density of 0.5 mA cm^{-2}, the capacitance is 106.4 mF cm^{-2}, and at the current densities of 1 mA cm^{-2}, 2 mA cm^{-2}, and 5 mA cm^{-2}, the specific capacitances were 99.2 mF cm^{-2}, 93.3 mF cm^{-2}, and 73.5 mF cm^{-2}, respectively (Fig. S11), showing high areal capacitance and good electrochemical performance.

Due to the limited energy and output power of a single supercapacitor, it is often difficult to meet diverse application requirements. Therefore, in order to be better used in practical working scenarios, a reasonable series–parallel design of the device is required (Fig. 4i). After connecting 2–4 devices in parallel, the current of the CV curve increases accordingly, while the voltage range remains the same (Fig. 4j). From Fig. 4k, whether 2, 3 or 4 devices are connected in parallel, the charge–discharge time is exactly 2 times, 3 times, and 4 times that of a single device. After connecting 4 devices in series, the voltage range is widened from 0.7 V to 2.8 V and the charging and discharging time after connecting 2–4 devices in series is basically consistent with that of a single device, with little difference (Fig. S12). The white LED can be successfully lit with the tandem hc-PANI based supercapacitors (Fig. 4l). Hence, the flexible supercapacitors prepared from hc-PANI have extremely

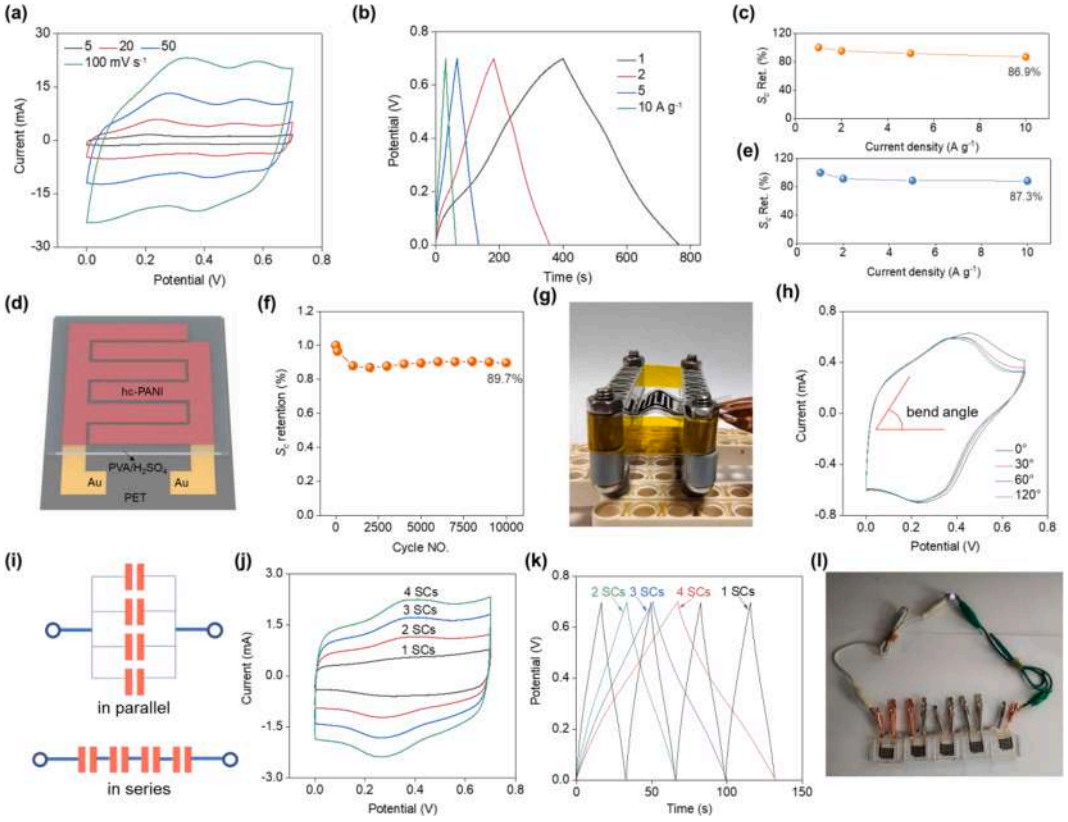

Fig. 4. The remarkable electrochemical properties of hc-PANI. (a-c) hc-PANI supercapacitor electrodes in a three-electrode configuration, (a) CV curve of 5 mV s^{-1}-100 mV s^{-1}, (b) GCD curves at current densities from 1 A g^{-1} to 10 A g^{-1}, (c) Rate-capability of hc-PANI. (d-h) hc-PANI based flexible supercapacitor device, (d) Schematic illustration of supercapacitors, (e) Rate-capability of hc-PANI based flexible supercapacitor device, (f) Capacitance retention after 10,000 cycles, (g) Schematic diagram of flexible test, (h) CV curves of hc-PANI flexible supercapacitors at different bending angles. (i-l) hc-PANI based multiple supercapacitors, (i) Sketch of four supercapacitor devices connected in parallel or in series, (j) CV curves of a single device and multiple devices in parallel, (k) GCD curves of a single device and multiple devices in parallel, (l) The tandem devices light the white LED lamp.

stable electrochemical performance and good uniformity, which can adapt to different voltage and current requirements of the range of applications.

4. Conclusion

In conclusion, the strategy of introducing copolymer was proposed to realize the construction of hyper-conjugated PANI with long conjugated chains. The introduction of 3-ABA is an essential key to form the additional hyper-conjugated effect through entering the PANI molecular chains and forming supramolecular hydrogen bonds. After introducing 3-ABA, hc-PANI also show a p-typed semiconducting behavior while the electrical conductivity is greatly increased by 800% in comparison with p-PANI, which is related to the smaller charge transfer energy barrier and is induced by an order of magnitude increment in the number of carriers. Because of hydrogen-bonding effect and hyper-conjugated effect, hc-PANI materials show a remarkable high specific capacitance of 521 F g^{-1} at 1 A g^{-1}, which is 50% higher than that of p-PANI. Moreover, hc-PANI based flexible supercapacitors share an 87.3% retention in specific capacitance as the current density increases to 10 A g^{-1}. After 10,000 cycles, they still have a capacitance retention of 89.7%, which can meet the needs of wearable electronics and other application fields.

Data availability

Data will be made available on request.

CRediT authorship contribution statement

Yihan Wang: Investigation, Formal analysis, Writing – original draft, Writing – review & editing. **Xiang Chu:** Methodology. **Hongrui Zhang:** Formal analysis. **Cheng Yan:** Formal analysis. **Guo Tian:** Formal analysis. **Weiqing Yang:** Funding acquisition, Resources. **Xiangrong Chen:** Resources. **Haitao Zhang:** Supervision, Conceptualization, Writing – original draft, Funding acquisition.

Declaration of Competing Interest

The authors declare that they have no known competing financial interests or personal relationships that could have appeared to influence the work reported in this paper.

Data availability

Data will be made available on request.

Acknowledgements

This work was supported by the National Natural Science Foundation of China (Nos. 51977185, 51972277), and the authors gratefully acknowledge the financial support from the Natural Science Foundation of Sichuan Province (No. 2023NSFSC0441).

Appendix A. Supplementary data

Supplementary data to this article can be found online at https://doi.org/10.1016/j.apsusc.2023.157350.

References

[1] S. Hou, L. Chen, X.L. Fan, X.T. Fan, X. Ji, B.Y. Wang, C.Y. Cui, J. Chen, C.Y. Yang, W. Wang, C.Z. Li, C.S. Wang, High-energy and low-cost membrane-free chlorine flow battery, Nat. Commun. 13 (2022) 1–8.
[2] W.H. Zuo, R.Z. Li, C. Zhou, Y.Y. Li, J.L. Xia, J.P. Liu, Battery-Supercapacitor Hybrid Devices: Recent Progress and Future Prospects, Adv. Sci. 4 (2017) 1600539.
[3] N.A. Kyeremateng, T. Brousse, D. Pech, Microsupercapacitors as miniaturized energy-storage components for on-chip electronics, Nat. Nanotechnol. 12 (2017) 7–15.
[4] L. Wang, X. Wang, J. Ouyang, Y. Guo, W. Xiong, L. Zhao, M. Li, Z. Hua, Z. Li, K. Du, C. Zhou, Y. Luo, Construction of polyaniline/MnO_2 core-shell nanocomposites in carbonized wood tracheids for high-performance all-solid-state asymmetric supercapacitors, Appl. Surf. Sci. 612 (2023), 155821.
[5] X. Wang, T.S. Mathis, K. Li, Z. Lin, L. Vlcek, T. Torita, N.C. Osti, C. Hatter, P. Urbankowski, A. Sarycheva, M. Tyagi, E. Mamontov, P. Simon, Y. Gogotsi, Influences from solvents on charge storage in titanium carbide MXenes, Nat. Energy 4 (2019) 241–248.
[6] V.S. Sumana, Y.N. Sudhakar, A. Varghese, G.K. Nagaraja, Pt nanoflower-poly (aniline) electrode material with the synchronized concept of energy storage in supercapacitor, Appl. Surf. Sci. 589 (2022), 152994.
[7] S. Yi, L. Wang, X. Zhang, C. Li, W.J. Liu, K. Wang, X.Z. Sun, Y.N. Xu, Z.X. Yang, Y. Cao, J. Sun, Y.W. Ma, Cationic intermediates assisted self-assembly two-dimensional $Ti_3C_2T_x$/rGO hybrid nanoflakes for advanced lithium-ion capacitors, Sci. Bull. 66 (2021) 914–924.
[8] X. Chu, Y. Wang, L. Cai, H. Huang, Z. Xu, Y. Xie, C. Yan, Q. Wang, H. Zhang, H. Li, W. Yang, Boosting the energy density of aqueous MXene-based supercapacitor by integrating 3D conducting polymer hydrogel cathode, SusMat 2 (2022) 379–390.
[9] J. Liu, D. Xuan, Z. Lu, Z. Wang, Q. Liu, S. Li, D. Wang, Y. Ye, D. Wang, Z. Zheng, A novel perspective on interfacial interactions between polypyrrole and carbon materials for improving performance of supercapacitors, Appl. Surf. Sci. 573 (2022), 151626.
[10] S. Choi, S.I. Han, D. Kim, T. Hyeon, D.H. Kim, High-performance stretchable conductive nanocomposites: materials, processes, and device applications, Chem. Soc. Rev. 48 (2019) 1566–1595.
[11] X. Chu, X. Zhao, Y.H. Zhou, Y.H. Wang, X.L. Han, Y.L. Zhou, J.X. Ma, Z.X. Wang, H. C. Huang, Z. Xu, C. Yan, H.T. Zhang, W.Q. Yang, J. Chen, An ultrathin robust polymer membrane for wearable solid-state electrochemical energy storage, Nano Energy 76 (2020), 105179.
[12] K.P. Liu, M.Y. Li, F.J. Zhang, Y.N. Wang, C. Chen, Y. Wei, L. Yang, R.F. Luo, Y. B. Wang, Chemical bonding of biological valve leaflets with an aminated zwitterionic copolymer for long-term anticoagulation and improved anti-calcification, Chem. Eng. J. 426 (2021), 131803.
[13] C. Choi, D.S. Ashby, D.M. Butts, R.H. DeBlock, Q.L. Wei, J. Lau, B. Dunn, Achieving high energy density and high power density with pseudocapacitive materials, Nat. Rev. Mater. 5 (2020) 5–19.
[14] H.L. Li, J.X. Wang, Q.X. Chu, Z. Wang, F.B. Zhang, S.C. Wang, Theoretical and experimental specific capacitance of polyaniline in sulfuric acid, J. Power Sources 190 (2009) 578–586.
[15] H.P. Cong, X.C. Ren, P. Wang, S.H. Yu, Flexible graphene-polyaniline composite paper for high-performance supercapacitor, Energ, Environ. Sci. 6 (2013) 1185–1191.
[16] L. Manjakkal, A. Pullanchiyodan, N. Yogeswaran, E.S. Hosseini, R. Dahiya, A Wearable Supercapacitor Based on Conductive PEDOT:PSS-Coated Cloth and a Sweat Electrolyte, Adv. Mater. 32 (2020) 1907254.
[17] Y. Liu, H. Zhou, W.X. Zhou, S. Meng, C. Qi, Z. Liu, T.T. Kong, Biocompatible, High-Performance, Wet-Adhesive, Stretchable All-Hydrogel Supercapacitor Implant Based on PANI@rGO/Mxenes Electrode and Hydrogel Electrolyte, Adv. Energy Mater. 11 (2021) 2101329.
[18] P. Song, X. He, J. Tao, X. Shen, Z. Yan, Z. Ji, A. Yuan, G. Zhu, L. Kong, H_2SO_4-assisted tandem carbonization synthesis of PANI@carbon@textile flexible electrode for high-performance wearable energy storage, Appl. Surf. Sci. 535 (2021), 147755.
[19] P.B. Liu, J. Yan, Z.X. Guang, Y. Huang, X.F. Li, W.H. Huang, Recent advancements of polyaniline-based nanocomposites for supercapacitors, J. Power Sources 424 (2019) 108–130.
[20] X. Chen, P.P. Liu, C.C. Liu, G.Q. Liu, J.L. Wei, J.K. Xu, Q.L. Jiang, X.F. Liu, F. X. Jiang, Microstructure control for high-capacitance polyaniline, Electrochim. Acta 391 (2021), 138977.
[21] P.P. Li, Z.Y. Jin, L.L. Peng, F. Zhao, D. Xiao, Y. Jin, G.H. Yu, Stretchable All-Gel-State Fiber-Shaped Supercapacitors Enabled by Macromolecularly Interconnected 3D Graphene/Nanostructured Conductive Polymer Hydrogels, Adv. Mater. 30 (2018) 1800124.
[22] W.W. Li, F.X. Gao, X.Q. Wang, N. Zhang, M.M. Ma, Strong and Robust Polyaniline-Based Supramolecular Hydrogels for Flexible Supercapacitors, Angew. Chem. Int. Edit. 55 (2016) 9196–9201.
[23] L.J. Pan, G.H. Yu, D.Y. Zhai, H.R. Lee, W.T. Zhao, N. Liu, H.L. Wang, B.C.K. Tee, Y. Shi, Y. Cui, Z.N. Bao, Hierarchical nanostructured conducting polymer hydrogel with high electrochemical activity, P. Natl. Acad. Sci. USA 109 (2012) 9287–9292.
[24] Y.H. Wang, X. Chu, Z.H. Zhu, D. Xiong, H.T. Zhang, W.Q. Yang, Dynamically evolving 2D supramolecular polyaniline nanosheets for long-stability flexible supercapacitors, Chem. Eng. J. 423 (2021), 130203.
[25] H.H. Zhou, M.Y. Ren, H.J. Zhai, Enhanced supercapacitive behaviors of poly(3,4-ethylenedioxythiophene)/graphene oxide hybrids prepared under optimized electropolymerization conditions, Electrochim. Acta 372 (2021), 137861.
[26] H.H. Zhou, Y.Q. Liu, M.Y. Ren, H.J. Zhai, Mechanically exfoliated graphite paper with layered microstructures for enhancing flexible electrochemical energy storage, Inorg. Chem. Front. 9 (2022) 1920–1930.
[27] J.L. Bredas, G.B. Street, Polarons, bipolarons, and solitons in conducting polymers, Accounts Chem. Res. 18 (1985) 309–315.
[28] M. Nowak, S.D.D.V. Rughooputh, S. Hotta, A.J. Heeger, Polarons and bipolarons on a conducting polymer in solution, Macromolecules 20 (1987) 965–968.

[29] Z. Zujovic, P.A. Kilmartin, J. Travas-Sejdic, The Applications of Solid-State NMR to Conducting Polymers, The Special Case on Polyaniline, Molecules 25 (2020) 444.
[30] R. Dilmurat, S. Prodhan, L.J. Wang, D. Beljonne, Thermally activated intra-chain charge transport in high charge-carrier mobility copolymers, J. Chem. Phys. 156 (2022), 084115.
[31] Q. Wang, K. Wang, C. Yan, X. Zeng, X. Fu, J. Cao, S. Yang, W. Li, X. Chen, W. Yang, Molecularly understanding and regulating carrier injection behavior of ETL/perovskite towards high performance PeLEDs, Chem. Eng. J. 456 (2023), 141077.
[32] X.D. Shehnaz, S.Z. Song, Y. Ren, Y.N. Yang, H.Y. Guo, Q. Jing, C. Mao, Hao, Polyaniline-based electrocatalysts through emulsion polymerization: Electrochemical and electrocatalytic performances, J. Energy Chem. 26 (2017) 182–192.
[33] D.D. Chen, X.H. Yi, C. Zhao, H.F. Fu, P. Wang, C.C. Wang, Polyaniline modified MIL-100(Fe) for enhanced photocatalytic Cr(VI) reduction and tetracycline degradation under white light, Chemosphere 245 (2020), 125659.
[34] S. Quillard, G. Louarn, S. Lefrant, A.G. Macdiarmid, Vibrational Analysis of Polyaniline - a Comparative-Study of Leucoemeraldine, Emeraldine, and Pernigraniline Bases, Phys. Rev. B 50 (1994) 12496–12508.
[35] M. Trchova, Z. Moravkova, J. Dybal, J. Stejskal, Detection of Aniline Oligomers on Polyaniline-Gold Interface using Resonance Raman Scattering, ACS Appl. Mater. Inter. 6 (2014) 942–950.
[36] L.P. Zhang, B. Wang, X.B. Li, G.P. Xu, S.L. Dou, X. Zhang, X. Chen, J.P. Zhao, K. Zhang, Y. Li, Further understanding of the mechanisms of electrochromic devices with variable infrared emissivity based on polyaniline conducting polymers, J. Mater. Chem. C 7 (2019) 9878–9891.
[37] J.P. Pouget, M.E. Jozefowicz, A.J. Epstein, X. Tang, A.G. MacDiarmid, X-ray structure of polyaniline, Macromolecules 24 (1991) 779–789.
[38] H.W. Park, T. Kim, J. Huh, M. Kang, J.E. Lee, H. Yoon, Anisotropic Growth Control of Polyaniline Nanostructures and Their Morphology-Dependent Electrochemical Characteristics, ACS Nano 6 (2012) 7624–7633.
[39] Y.Z. Li, X. Zhao, Q. Xu, Q.H. Zhang, D.J. Chen, Facile Preparation and Enhanced Capacitance of the Polyaniline/Sodium Alginate Nanofiber Network for Supercapacitors, Langmuir 27 (2011) 6458–6463.
[40] C.C. Zhang, F.M. Allioux, M.A. Rahim, J.L. Han, J.B. Tang, M.B. Ghasemian, S. Y. Tang, M. Mayyas, T. Daeneke, P. Le-Clech, R.B. Kaner, D. Esrafilzadeh, K. Kalantar-Zadeh, Nucleation and Growth of Polyaniline Nanofibers onto Liquid Metal Nanoparticles, Chem. Mater. 32 (2020) 4808–4819.
[41] S. Chen, D.L. Huang, G.M. Zeng, W.J. Xue, L. Lei, P. Xu, R. Deng, J. Li, M. Cheng, In-situ synthesis of facet-dependent BiVO4/Ag3PO4/PANI photocatalyst with enhanced visible-light-induced photocatalytic degradation performance: Synergism of interfacial coupling and hole-transfer, Chem. Eng. J. 382 (2020), 122840.
[42] M.M. Mahat, D. Mawad, G.W. Nelson, S. Fearn, R.G. Palgrave, D.J. Payne, M. M. Stevens, Elucidating the deprotonation of polyaniline films by X-ray photoelectron spectroscopy, J. Mater. Chem. C 3 (2015) 7180–7186.
[43] Y. Cao, S. Li, Z. Xue, D. Guo, Spectroscopic and electrical characterization of some aniline oligomers and polyaniline, Synthetic Met. 16 (1986) 305–315.
[44] M. Sommer, S.M. Lindner, M. Thelakkat, Microphase-Separated Donor-Acceptor Diblock Copolymers: Influence of HOMO Energy Levels and Morphology on Polymer Solar Cells, Adv. Funct. Mater. 17 (2007) 1493–1500.
[45] N. Ueno, S. Kera, K. Sakamoto, K.K. Okudaira, Energy band and electron-vibration coupling in organic thin films: photoelectron spectroscopy as a powerful tool for studying the charge transport, Appl. Phys. A-Mater. 92 (2008) 495–504.
[46] M.T. Chen, O.T. Hofmann, A. Gerlach, B. Broker, C. Burker, J. Niederhausen, T. Hosokai, J. Zegenhagen, A. Vollmer, R. Riegel, K. Mullen, F. Schreiber, I. Salzmann, N. Koch, E. Zojer, S. Duhm, Energy-level alignment at strongly coupled organic-metal interfaces, J. Phys-Condens. Mat. 31 (2019), 194002.
[47] J. Sworakowski, How accurate are energies of HOMO and LUMO levels in small-molecule organic semiconductors determined from cyclic voltammetry or optical spectroscopy? Synthetic Met. 235 (2018) 125–130.
[48] S. Pu, Z.X. Wang, Y.T. Xie, J.T. Fan, Z. Xu, Y.H. Wang, H.Y. He, X. Zhang, W. Q. Yang, H.T. Zhang, Origin and Regulation of Self-Discharge in MXene Supercapacitors, Adv. Funct. Mater. 33 (2023) 2208715.
[49] X.L. Jiang, X. Chu, X. Zhang, Y.T. Xie, T. Yang, J.F. Huang, W. Li, W.L. Deng, H. T. Zhang, W.Q. Yang, Surplus charge injection enables high-cell-potential stable 2D polyaniline supercapacitors, Electrochim. Acta 445 (2023), 142052.
[50] G.M. Liu, W. Jaegermann, J.J. He, V. Sundstrom, L.C. Sun, XPS and UPS characterization of the TiO_2/ZnPcGly heterointerface: Aligmment of energy levels, J. Phys. Chem. B 106 (2002) 5814–5819.
[51] P. Wang, F. Shao, B. Li, Y. Su, Z. Yang, N. Hu, Y. Zhang, Molecular-level uniform graphene/polyaniline composite film for flexible supercapacitors with high-areal capacitance, Nanotechnology 34 (2023).
[52] T.Y. Dai, Y.J. Jia, Supramolecular hydrogels of polyaniline-poly(styrene sulfonate) prepared in concentrated solutions, Polymer 52 (2011) 2550–2558.
[53] Q. Wu, Y.X. Xu, Z.Y. Yao, A.R. Liu, G.Q. Shi, Supercapacitors Based on Flexible Graphene/Polyaniline Nanofiber Composite Films, ACS Nano 4 (2010) 1963–1970.
[54] L. Li, Y. Zhang, H. Lu, Y. Wang, J. Xu, J. Zhu, C. Zhang, T. Liu, Cryopolymerization enables anisotropic polyaniline hybrid hydrogels with superelasticity and highly deformation-tolerant electrochemical energy storage, Nat. Commun. 11 (2020) 62.
[55] V.S. Patil, S.S. Thoravat, S.S. Kundale, T.D. Dongale, P.S. Patil, S.A. Jadhav, Synthesis and testing of polyaniline grafted functional magnetite (Fe_3O_4) nanoparticles and rGO based nanocomposites for supercapacitor application, Chem. Phys. Lett. 814 (2023), 140334.